TECHNICAL MEMORANDUM

715

SMOS brightness temperatures angular noise: characterization, filtering and validation.

J. Muñoz Sabater,
P. de Rosnay, C. Jiménez,
L. Isaksen and C. Albergel

Research Department

IEEE Transactions on Geoscience and Remote Sensing. Accepted.

November 2013

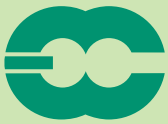

European Centre for Medium-Range Weather Forecasts
Europäisches Zentrum für mittelfristige Wettervorhersage
Centre européen pour les prévisions météorologiques à moyen terme

Series: ECMWF Technical Memoranda

A full list of ECMWF Publications can be found on our web site under:
http://www.ecmwf.int/publications/

Contact: library@ecmwf.int

European Centre for Medium-Range Weather Forecasts
Shinfield Park, Reading, RG2 9AX, England

Abstract

The 2D-interferometric radiometer on board SMOS has been providing a continuous dataset of brightness temperatures, at different viewing geometries, containing information of the Earth's surface microwave emission. This dataset is affected by several sources of noise, which are a combination of the noise associated with the radiometer itself and the different views under which a heterogeneous target, such as continental surfaces, is observed. As a result, the SMOS dataset is affected by a significant amount of noise. For many applications, as soil moisture retrieval, reducing noise from the observations while keeping the signal is necessary, and the accuracy of the retrievals depends on the quality of the observed dataset. This paper investigates the averaging of SMOS brightness temperatures in angular bins of different size as a simple method to reduce noise. All the observations belonging to a single pixel and satellite overpass were fitted to a polynomial regression model, with the objective of characterizing and evaluating the associated noise. Then the observations were averaged in angular bins of different size and the potential benefit of this process to reduce noise from the data was quantified. It was found that if a 2-degree angular bin is used to average the data, the noise is reduced by up to 3 K. Furthermore, this method complements necessary data thinning approaches when a large volume of data is used in data assimilation systems.

1 Introduction

The Soil Moisture and Ocean Salinity (SMOS) satellite of the European Space Agency (ESA), launched in November 2009, is providing a large amount of data sensitive to soil moisture over continental surfaces (1). The instrument on board the SMOS platform is the Microwave Imaging Radiometer by Aperture Synthesis (MIRAS). This is the first time that a 2D-interferometric radiometer is being used to measure soil moisture and ocean salinity from a space sensor. The cross-correlation of the signal collected by a series of antennas equally distributed along three arms makes it possible to provide observations with a spatial resolution between 35 and 50 km over continental surfaces and a target accuracy of $0.04 m^3 m^{-3}$ (2; 3; 1).

The challenges the SMOS mission face are multiple. Not only is a new instrument being tested, but also a new type of observation. SMOS provides multi-angular measurements of polarised brightness temperatures, i.e. a region on the Earth's surface is being observed under different viewing angles producing different pixel sizes and orientations, as well as different noise and precision for each pixel (2). Depending on the location of the observed area within the Field Of View (FOV), the number of views can vary up to 160. The observed areas furthest from the centre of the ground track are sampled fewer times than those located near the centre. The geometry of the observation is complex; a complete image of the surface emission is produced by inverting the visibilities associated to the interferometric technique (4). Errors in the reconstructed image should be expected due to inaccuracies in the antenna pattern estimation, the Noise Injection Radiometers' (NIR) brightness temperature measurements (5) and the algorithm which reconstructs the image. The latter is as a first approximation an inverse Fourier transform (6) or a more sophisticated G-matrix inversion ((7; 8)), with a potential degradation of the radiometric sensitivity in terms of a higher noise. Another source of noise is the radiometer itself. Any imaging radiometer, in fact, is affected by three types of noise (9): a) the radiometric resolution (temporal standard deviation of the zero-mean random error due to the finite integration time) (10), b) the radiometric bias (spatial average of all the systematic errors) and c) the radiometric accuracy (spatial standard deviation of the sum of all the systematic errors (11)). Although these sources of noise are linked to the instrumentation and measurement technique used for SMOS, another new potentially large source of noise is embedded in the measurements. In SMOS, the same area of the Earth's surface can be observed under different viewing geometries, and that can turn into quite different pixel shapes and sizes, especially at large incidence angles. This implies that even at slightly different viewing angles, the surface contribution to the

final observation value can arise from very different areas and land cover types, all of them with very different emission properties. This is especially important when looking at inhomogeneous targets, such as the Earth's surface. Therefore, a significant angular noise contribution is expected due to the strong inhomogeneities of the Earth's continental surfaces.

This paper aims at; (i) characterizing the angular noise of SMOS brightness temperatures. To this end, the observations were fitted to a polynomial regression model, which was used as a reference model of the observations angular distribution, (ii) filtering noise of the observed dataset, while still retaining the signal. For this purpose, a simple method consisting in averaging SMOS brightness temperatures in angular bins of different size is proposed and tested, and (iii) validate the effectiveness of angular binning the data to filter noise. For that, the same type of polynomial regression model employed to characterize the noise of the observations, was used. Applications which use SMOS brightness temperatures, such as soil moisture retrievals, drought monitoring or Numerical Weather Predictions (NWP) systems, benefit from filtering noise of the original dataset. For NWP applications, noise filtering forms part of a set of preprocessing activities (such as bias correction, thinning, quality control) ensuring that data assimilation systems make optimal use of satellite and model data. Indeed, any data assimilation system aims at assimilating only observations of high quality, carrying signal rather than noise. They are able to use observations more effectively if noise is removed at this stage. Furthermore, angular binning the data is computationally affordable and simple enough to be implemented in a complex NWP system, such as the Integrated Forecasting System (IFS) of the European Centre for Medium-Range Weather Forecasts (ECMWF). As pointed out by (12), the implementation of SMOS data in the IFS is a big challenge and methods that reduce complexity are preferable.

After the description of the observations used in this study (section 2.1), the methodology employed to investigate the noise affecting the observations and the benefits of averaging the data in angular bins is described (sections 2.2 and 2.3) and analysed (section 3). The sensitivity of the noise affecting the observations to different types of soil texture and vegetation cover, as well as to the incidence angle and the radiometric accuracy of the observations, is also investigated in section 4. In section 5 a case study shows the benefits of binning the data as input in a real analysis experiment. Finally, section 6 provides a brief summary of the methodology presented in this paper and the most important conclusions.

2 Material and Methods

2.1 Observations

The product used at ECMWF is the near-real-time (NRT) brightness temperatures. It is a reprocessed sub-product of level-1b data and they differ from the latter in that they are geographically sorted swath-based maps of brightness temperature. The geolocated product received at ECMWF is arranged in an equal-area grid system called ISEA 4H9 (Icosahedron Snyder Equal Area grid with Aperture 4 at resolution 9) (13). For this grid, the centres of the cell grids are at equal distance of 15 km with a standard deviation of 0.9 km. This constitutes the SMOS Discrete Global Grid (DGG). This fine grid has been adopted in order to provide the correct sampling for the measurements at a spatial resolution of 30 Km according to the Nyquist criteria (14).

The data is organized in messages. Each message corresponds to a snapshot where the integration time is 1.2 seconds, as this is the time in which all correlations of a single scene are measured. Each snapshot contains a number of subsets, each providing an observation at a node of the ISEA grid. On average, each snapshot contains more than 4500 subsets if the instrument runs in dual-polarisation mode. In this running mode, dataset records are generated each 1.2 seconds at the XX and YY polarisations alternately. In full-polarisation mode (current operational mode) all receivers in the three arms are in the

same polarisation for the first integration, whereas in the next integration the receivers in an arm switch the polarisation and two dataset records are generated, thus doubling the information per snapshot. The NRT product reaches ECMWF archives with a few hours of delay since after the sensing time. This makes it possible to ingest the data in the IFS soon after they are generated, to enable SMOS brightness temperatures to be monitored operationally and produce first-guess departures (12). It also opens the possibility to produce an NRT soil moisture analysis.

2.2 Angular noise characterization and validation strategy

The natural emission of the soil in the lower-frequency microwave domain depends on several surface variables. In general, for electromagnetic waves polarised horizontally, the observed brightness temperatures decrease as the incidence angle increases, whereas the opposite behaviour is observed for the vertically polarised component. The ratio of increase or decrease with the incidence angle depends critically on the soil state (soil moisture, soil temperature), type of vegetation cover and soil properties (soil roughness, soil texture, density of the vegetation canopy, etc.). However, as a first-order approximation, the angular signature of a target at a given time can be characterized by a n^{th} order polynomial. In this study only polynomials of second and third order were used. The method employed here to validate the angular binning approach consists in fitting all the observations of the same SMOS DGG node (corresponding to spatially averaged values centered on the node) and orbit to polynomials of 2^{nd} and 3^{rd} order. If the polynomial regression model is a good representation of the observed brightness temperature distribution, then the coefficient of determination (r^2) will have a high value. r^2 explains what percent of the total brightness temperature variance is explained by the polynomial regression model, and varies from 0 to 1. The remaining variance ($1\text{-}r^2$) is the variability of the observations from the regression model. The standard deviation of the residues to the fitted curve (STD) provides an approximate indication of the noise associated with the observations. Averaging the observations in angular bins of different size is expected to reduce the residues to the fitted curve and hence the noise associated with different viewing geometries. Note that the polynomial fit does not lead to noise filtering or to derive any angular relationship, but is just a tool used here to validate the binning approach as a practical way of reducing noise, while retaining the signal of the data. As an indirect thinning scheme, binning the data also reduces the number of entries for assimilation. The added value compared to early thinning strategies ((15; 12)) is that it avoids excluding useful data at early stages. This simple validation strategy can be used under the following considerations:

a) As brightness temperatures measured at the top of the atmosphere are very sensitive to the geophysical characteristics and meteorological conditions of the soil (soil moisture, temperature, vegetation cover, surface roughness, etc.), the polynomial fit will be representative of these observations only if measurements acquired during a single orbit pass are considered. Otherwise, the natural geophysical variability of the signal could be embedded in the estimated level of noise of the observations. For example, if over a certain target it rains between two satellite passes, the observed brightness temperatures will be very different, thus mixing natural variability and noise of the signal. If several orbits are to be used, then areas which have demonstrated to be very stable in time (e.g. Antarctic, a desert) may be used.

b) In order to avoid contamination of the signal due to Radio Frequency Interference (RFI), only Australia, South America and North America were analysed separately in this study. Although these continents are not free from RFI, at least the RFI effect is less serious than over Europe and Asia.

c) Averaging over relatively small angular bins should be acceptable to reduce observational noise due to surface heterogeneities, but over large bins (5 degrees or more) this method could mistakenly not only reduce the random nature of the noise affecting the observations, but also the natural variability of the signal, because brightness temperatures can change significantly with the incidence angle (specially for

large incidence angles).
d) The data used in this study are not reprocessed data (not available at the time of the study); however, this is not an issue as in this paper only orbits contained in 24 h and two contrasted seasons were considered.
Based on the above considerations, data acquired during two single days representing two different seasons were selected: 1 December 2010 and 1 June 2011. In particular, two ECMWF analysis cycles of 12 h (as in the operational suite) were used, so data analysed is from 21 h UTC on 30 November 2010 to 21 h UTC on 1 December 2010, and from 21 h UTC on 31 May 2011 to 21 h UTC on 1 June 2011 (16). Tests with more recent data and different orbits were also carried out, but the conclusions found in this paper were similar. Each observation was quality checked as in (12). Ascending and descending orbits were analysed separately, as well as XX and YY polarisations. Firstly, all the observed brightness temperatures recorded over the same node of the SMOS DGG grid, and for the same polarisation and type of orbit, were fitted to polynomials of 2^{nd} and 3^{rd} order. The minimum number of observations per node necessary to compute a fit was arbitrarily set to 10. This criterion excluded between 25 to 35% of nodes (with incidence angles mostly comprised between 42 and 48 degrees). However, the population of each incidence angle was well represented in the total average. Larger bin sizes were avoided because there is a risk of mixing the angular natural variability of the observations, specially for large incidence angles where the angular gradient can be very large. In order to consider only significant correlations, the Pearsons coefficient with 5% significance level was evaluated at each time. In this case, configurations where the p-value was larger than 0.05 were rejected and not accounted for in the statistics, as the correlation value is from the statistical point of view a pure coincidence (17). Then the mean r^2 and STD per continent were analysed for all the different cases, as examined in section 3.

2.3 Pre-analysis of singular grid points

Several nodes of the SMOS DGG grid representing different soil conditions (bare soil, dense forest, soil covered by a shallow layer of snow, soil covered by a large amount of snow and a coastal node) were chosen for a specific day. The aim was to understand the characteristic behaviour in one dimension of the brightness temperatures as a function of the incidence angle for these soil conditions, and how averaging the data in angular bins could affect this behaviour. This will support the interpretation of global maps. The validation strategy described in section 2.2 was applied to these nodes. Fig. 1 shows the geographical location of the selected points. Fig. 2 shows all the observations collected for each of these grid points (as crosses) and overlapped on them is the 2^{nd}-order polynomial fitted curve using all the observations (left panel) and a 2-degree angular averaging (right panel), for the YY polarisation. This figure shows that under bare soil (top panel), the regression curve fits the observations very well, reducing the residues from 4.5 K when all the observations were used to 2.6 K when a 2-degree angular bin was used. It also shows sensitivity to the incidence angle (between 70 and 60 K using all the observations or a 2-degree angular bin, respectively). For dense canopies a weak sensitivity of brightness temperatures with the incidence angle should be expected. Indeed, the signal is much flatter due to the masking effect and the emission of the vegetation canopy itself at all incidence angles (Figs. 2c and d). For this type of surface, averaging the data in angular bins does not significantly reduce the residues to the polynomial fit. The effect of snow on the L-band emission depends on many variables, as the granularity, density, depth or age, but even wet and dry snow have different dielectric properties. That makes Figs. 2e to Fig. 2h to present a noisier angular distribution. Note that shallow and deep snow were arbitrarily defined: less than 20 cm shallow snow, more than 20 cm deep snow. Although, in both cases, averaging the data in bins of 2 degrees seems to be relatively effective, this type of grid point will be rejected in an assimilation context as the sensitivity to soil moisture is lost and not well known. Grid points near the coast present

the highest noise due to the mixed area of land and ocean signal in the same observation (Figs. 2i and 2j). In this case, the polynomial regression model did not fit the observations well.

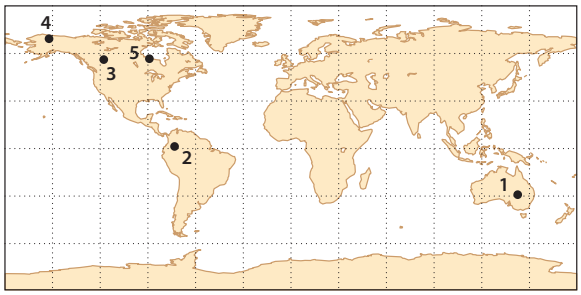

Figure 1: Location of the single points analysed in section III-B. Their geographical coordinates are displayed with the format [lat/lon]; (1) bare soil [-29.017,143.003], (2) dense forest [1.279,-73.565], (3) shallow snow layer [56.319,-117.879] (based on 6 cm snow depth forecast), (4) deep snow layer [69.599,-151.914] (based on 73 cm snow depth forecast) and (5) coastal node [56.765,-89.018] (located at approximately 3 miles of the Hudson Bay).

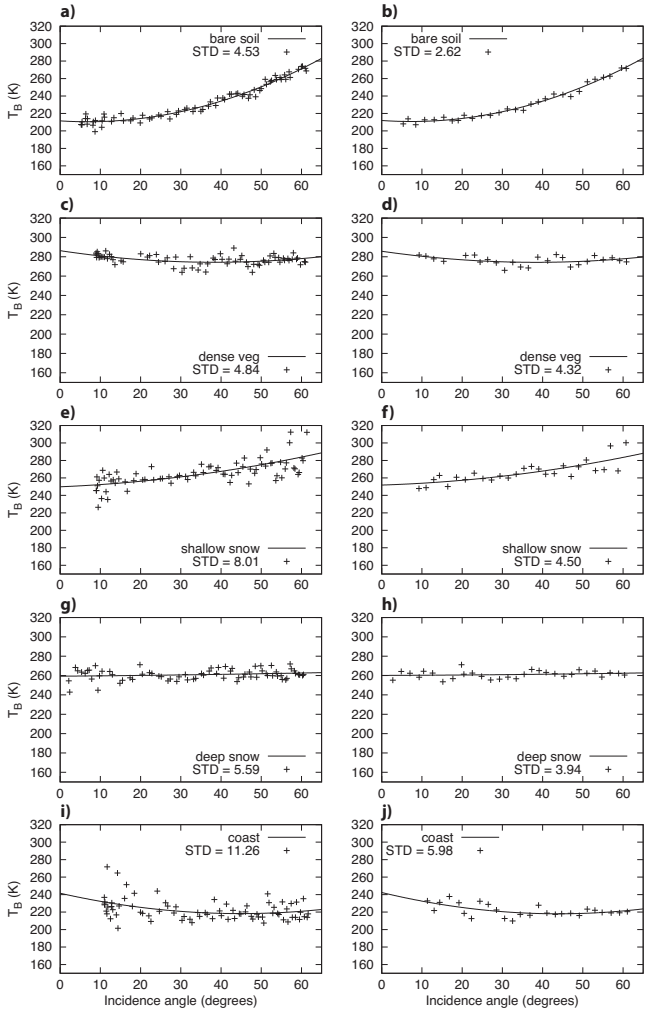

Figure 2: 2nd-order polynomial fitted curve (solid line) to all observations (left panel) and to observations averaged in a bin of 2 degrees (right panel) for the YY polarisation. T_B is the brightness temperatures of the observations, and STD is the standard deviation of the residues to the fitted curve.

3 Noise filtering and validation results

3.1 Qualitative analysis

The left panel of Fig. 3 shows the r^2 maps of SMOS brightness temperatures fitted to a 2^{nd}-order polynomial regression model, for the different angular bins used in this study, for XX polarisation and ascending orbits over Australia, on 1 December 2010. Each r^2 value was computed individually for each node of the SMOS DGG. The right panel of Fig. 3 shows the equivalent maps of the variability of the residues (STD) to the fitted curve. Equivalent maps (not shown) were obtained for North America and South America, for ascending and descending passes, for both polarisations and also for the June case. As an example, Fig. 4 shows the equivalent maps for South America and for YY polarisation and descending orbits, and Fig. 5 is for North America, XX polarisation and ascending orbits, but for the sake of simplicity only the maps using all the observations and only 2-degree bins are shown. The analysis of all these maps shows the following features:

(a) As expected, the edges of the satellite track are the most noisy areas of the FOV. This can be clearly observed in Fig. 3a, where all the observations were used, because there was a poor fit of the observations to the polynomial curve at the edges of the ground track and large STD. The polynomial regression model is not a good representation of this area of the FOV, which is quite noisy. Indeed, the limits of the (extended) alias-free zone are due to replicas of the Earth visibility zone (18), and therefore of lower quality. This low-performance area is the extended-alias FOV (EA-FOV), and mostly contains incidence angles greater than 45 degrees. If an insufficient number of observations were available within an angular bin to carry out a regression fit, then this grid point was filtered out and not included in the statistics. This explains the fact that as the size of the angular bin increases (and therefore a lower number of available observations), the ground track gets progressively smaller, as shown in Figs. 3g to 3j.

(b) The behaviour near the coastline is very different for the two polarisations analysed here. Whereas the XX polarisation shows very high correlation with the regression model near the coastlines, the opposite behaviour is found for YY polarisation (see for instance Fig. 4 for YY polarisation in contrast to Fig. 5 for XX polarisation). This behaviour is common for both ascending and descending orbits. By increasing the incidence angle of the observations, larger areas contribute to the signal, and near the coast this means, in many cases, a larger contribution of the sea surface to the signal (which is a weaker signal). While the XX polarisation behaves as theoretically expected, the signal of the YY polarisation stays quite noisy and flat instead of growing with the incidence angle. This effect is a combination of the proximity to oceans (which compensates for an increase in brightness temperature with increasing incidence angle) and a lower sensitivity to water bodies.

(c) It was also found that the angular signature in areas covered by snow (see Fig. 5) presents large noise, as was also shown in section 2.3. For these grid points the correlation of the polynomial regression model to the observations is very poor, and worse for YY polarisation than for XX polarisation. Snow characteristics present a large variation in time and space, with strong variations in terms of solid and liquid water content, as well as in snow cover area. These strong heterogeneities contribute to increase the noise of the angular signal. The YY polarisation presents flatter angular signals and, therefore, the presence of noise quickly reduces the correlation with a relatively flat curve. The same behaviour occurs for very dense forests such as the Amazon, but in this case some areas present stronger noise at the XX polarisation. These areas present flat angular signatures and the presence of noise also causes the coefficient of determination to be reduced quickly.

(d) In general it was found that a 2^{nd}-order polynomial represents better the angular behaviour of the observations in the XX polarisation than in the YY polarisation, because the latter has a lower angular sensitivity to soil moisture. A quantitative analysis can be found in section 3.2.

(e) The December and June cases showed equivalent results. Some geographical changes are mainly

found in North America, which is due to the differences in the area covered by snow. A 2^{nd}-order polynomial regression model should not be used as a reference model when snow or dense canopies are present. In any case, for assimilation experiments these types of surface cover will be flagged and rejected, as the sensitivity to soil moisture is masked or unknown.

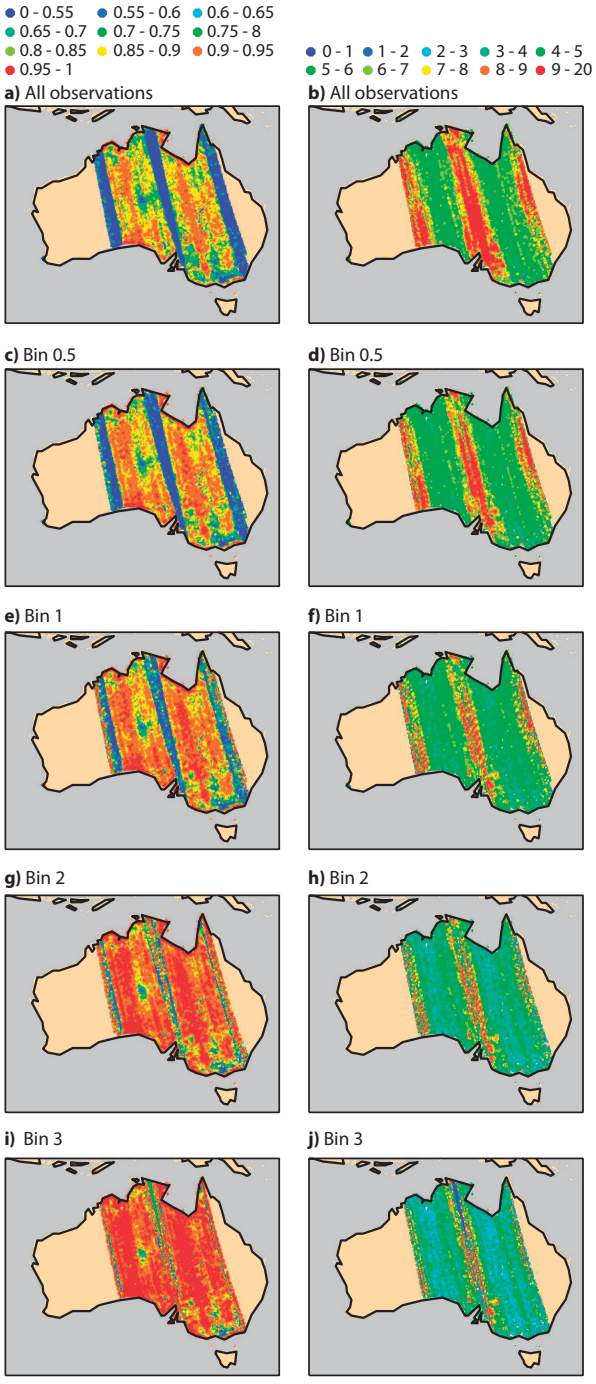

Figure 3: Coefficient of determination (r^2, left panel) and STD of the residues (in K, right panel) between the SMOS brightness temperature angular signature and its 2^{nd}-order polynomial regression model for the XX polarisation and ascending orbits, on 1 December 2010. In a) and b) all the observations are used (no binning), whereas observations are averaged in a bin of 0.5 degrees (c,d), 1 degree (e,f), 2 degrees (g,h), and 3 degrees (i,j).

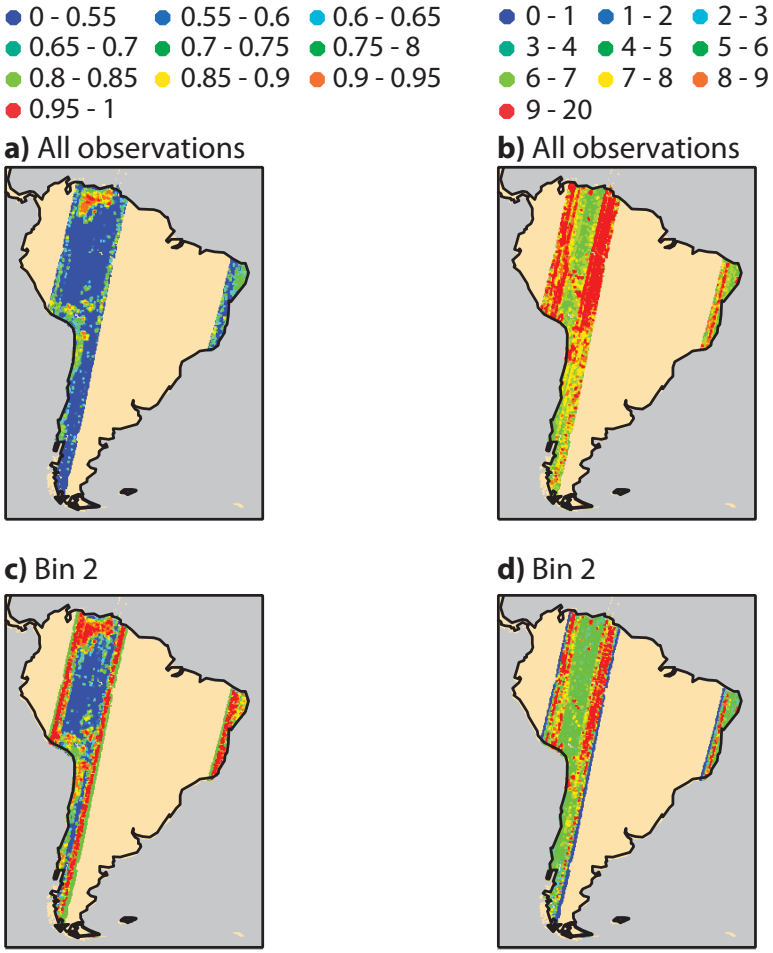

Figure 4: As Fig. 3, but for South America, YY polarisation and descending orbits. In a) and b) all the observations are used (no binning), whereas in c) and d) observations are averaged in a bin of 2 degrees.

3.2 Quantitative analysis

The mean value of the r^2 and the STD statistical variables were computed independently for each continent, type of orbit, polarisation, bin size and type of regression model, as explained in section 2.2. Only significant correlations were considered (p-value lower than 0.05 (17)). Table 1 presents the mean statistics, by fitting the observations to a 2^{nd} and 3^{rd}-order polynomial, on 1 December 2010 for Australia, North America and South America, respectively. Table 2 shows the same averaged values for 1 June 2011, but only using as regression model a 2^{nd}-order polynomial function. It was found that: (a) The STD of the residues to the fitted curve consistently decreases as the size of the angular bin increases. For the winter case, without any binning the continental averaged noise of the observations varies from 5.4 K to 6.4 K using a 2^{nd}-order polynomial regression model, and from 5.6 K to 7.1 K using a 3^{rd}-order polynomial. If a 3-degree maximum bin size is used, these values fluctuate from 2.3 K to 2.8 K (with a 2^{nd}-order polynomial) and from 2.5 K to 2.8 K (with a 3^{rd}-order polynomial). The June case shows very similar results, except for the ascending orbits of North America, which show larger noisy values. According to Tables 1 and 2, in a significant amount of cases a potential noise reduction larger than 3 K could be achieved by averaging the observations in bins up to 3 degrees. However, in 86% of cases (and all of the summer cases), averaging the observations in bins of 3 degrees did not result in better r^2 than

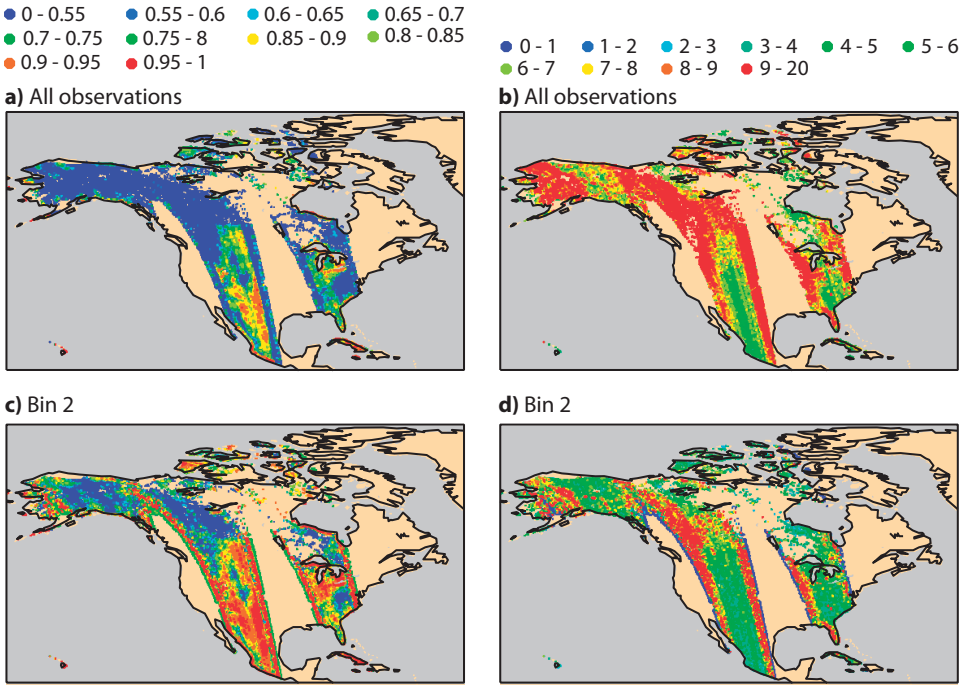

Figure 5: As Fig. 3, but for North America. In a) and b) all the observations are used (no binning), whereas in c) and d) observations are averaged in a bin of 2 degrees only.

for bins of 2 degrees. Indeed, in most cases 3-degree averaging is worse. This is an indication that when excessively large bins are applied the natural variability of the observations is included, and thus the polynomial fit is no longer a better representation of the observations. Higher-order polynomials change the sign of the gradient several times and they have the potential to fit better the noise, which is not the objective of the methodology presented in this paper. Therefore, averaging the observations in bins of 2 degrees should be the maximum acceptable to reduce noise from the observations. It was checked (not shown) that with larger angular bins (4, 5 and 6 degrees) the r^2 became slightly worse. Hereafter, only a 2^{nd}-order polynomial regression model will be used for further analysis.

(b) In most of the cases studied, the polynomial fit represents better the XX polarisation than the YY polarisation, except for some orbits over South America where the behaviour is found to be more alike. Likewise, the STD is, in general, also lower for the XX mode than for the YY mode. Although the XX polarisation is more sensitive to the soil water content and shows greater dynamics ((19)), these results suggest that a stronger dynamical signal does not necessarily involve a larger associated noise. After averaging the observations in angular bins of 2 degrees, the noise difference between XX and YY polarisations is lower than 1 K, often less than 0.5 K, except for the ascending case over North America, where the difference is 1.16 K. Again, this is due to the higher sensitivity of the snow water content of the XX polarisation, which produces larger differences between the two polarisation modes used in this study.

(c) While the STD of the residues is larger in ascending than in descending orbits, the trend is that the polynomial regression model explains better the distribution of brightness temperatures for ascending orbits. However, these results change for continent, polarisation and period of the year. For Australia and South America, in general, r^2 is better for ascending than for descending orbits; however, descending orbits show lower STD. The North America case seems to be more dependent on the period of the year, which is associated with the snow covered area during the winter period. In this case, the r^2 values are significantly higher for the YY polarisation in the June case.

Table 1: Mean r^2 and STD (in K) between the SMOS observed brightness temperature angular signature and its 2^{nd} and 3^{rd}-order polynomial fitted curve, for Australia, North America and South America on 1 December 2010.

		model: Ax^2+Bx+C								model: Ax^3+Bx^2+Cx+D							
		ASCENDING				DESCENDING				ASCENDING				DESCENDING			
		XX		YY		XX		YY		XX		YY		XX		YY	
	bin	r^2	STD	r^2	STD	r^2	STD	r^2	STD	r^2	STD	r^2	STD	r^2	STD	r^2	STD
Australia	no-bin	0.65	5.16	0.56	6.23	0.58	4.65	0.48	5.46	0.68	5.39	0.61	6.39	0.63	4.98	0.55	5.63
	0.5	0.66	4.33	0.59	5.21	0.59	3.91	0.51	4.61	0.71	4.56	0.66	5.36	0.65	4.27	0.59	4.82
	1	0.70	3.80	0.63	4.45	0.63	3.38	0.55	3.91	0.75	3.95	0.70	4.54	0.70	3.61	0.63	4.02
	2	0.73	3.10	0.66	3.54	0.63	2.55	0.56	2.94	0.77	3.13	0.71	3.52	0.65	2.58	0.58	2.87
	3	0.73	2.73	0.66	2.98	0.61	2.14	0.53	2.40	0.73	2.65	0.68	2.87	0.60	2.06	0.55	2.26
North America	no-bin	0.40	5.89	0.32	8.15	0.42	5.42	0.32	6.07	0.45	6.56	0.37	9.16	0.47	5.85	0.38	6.65
	0.5	0.43	4.87	0.35	6.80	0.45	4.46	0.35	4.89	0.49	5.48	0.42	7.67	0.52	4.80	0.43	5.44
	1	0.48	4.18	0.40	5.76	0.50	3.81	0.39	4.10	0.55	4.60	0.48	6.40	0.57	4.04	0.48	4.52
	2	0.51	3.10	0.45	4.26	0.53	2.89	0.44	3.09	0.56	3.32	0.50	4.59	0.57	2.96	0.50	3.31
	3	0.52	2.54	0.46	3.34	0.53	2.41	0.45	2.53	0.54	2.64	0.50	3.60	0.55	2.42	0.50	2.67
South America	no-bin	0.41	7.06	0.42	6.09	0.33	5.21	0.28	4.68	0.47	7.87	0.49	6.40	0.40	5.62	0.37	5.51
	0.5	0.43	5.95	0.44	5.12	0.35	4.42	0.29	3.80	0.50	6.75	0.52	5.52	0.44	4.83	0.41	4.68
	1	0.47	4.96	0.48	4.30	0.40	3.77	0.33	3.13	0.55	5.61	0.56	4.63	0.48	4.02	0.45	3.83
	2	0.48	3.57	0.50	3.22	0.40	2.62	0.32	2.19	0.53	3.96	0.55	3.36	0.44	2.80	0.40	2.66
	3	0.47	2.83	0.48	2.60	0.38	2.08	0.30	1.69	0.50	3.15	0.53	2.69	0.41	2.18	0.36	2.04

Table 2: Mean r^2 and STD (in K) between SMOS observed brightness temperature angular signature and its 2^{nd}-order polynomial fitted curve, for Australia, North America and South America, on 1 June 2011.

model: $Ax^2 + Bx + C$

		ASCENDING				DESCENDING			
		XX		YY		XX		YY	
	bin	r^2	STD	r^2	STD	r^2	STD	r^2	STD
Australia	no-bin	0.63	4.64	0.50	5.55	0.59	4.65	0.52	5.63
	0.5	0.64	3.93	0.53	4.72	0.60	3.89	0.54	4.78
	1	0.68	3.38	0.57	4.00	0.65	3.32	0.59	3.98
	2	0.68	2.60	0.59	3.08	0.64	2.46	0.59	3.01
	3	0.66	2.22	0.57	2.51	0.60	2.07	0.55	2.43
North America	no-bin	0.30	11.44	0.26	14.11	0.46	5.79	0.45	6.53
	0.5	0.33	8.77	0.29	10.94	0.48	4.91	0.48	5.51
	1	0.38	6.91	0.34	8.56	0.53	4.23	0.52	4.63
	2	0.41	4.81	0.37	5.56	0.56	3.18	0.56	3.52
	3	0.41	3.76	0.37	4.33	0.56	2.64	0.56	2.91
South America	no-bin	0.44	5.32	0.36	5.52	0.37	6.49	0.39	6.44
	0.5	0.46	4.54	0.38	4.67	0.39	5.54	0.41	5.43
	1	0.51	3.94	0.41	3.95	0.44	4.81	0.45	4.60
	2	0.53	2.98	0.43	2.92	0.46	3.61	0.48	3.55
	3	0.52	2.50	0.43	2.33	0.45	2.98	0.47	2.91

4 Sensitivity to soil texture, vegetation cover type, incidence angle and radiometric accuracy

4.1 Sensitivity to soil texture

The potential influence of the soil texture on the angular signature of the observations was also investigated. Mean statistics were computed independently, separating the observations over each type of soil texture used in the land surface module of the IFS model, H-TESSEL (20). According to this classification, up to seven different soil textures types are allowed (coarse, medium, medium-fine, fine, very fine, organic and tropical organic), all of them with their own wilting point and field capacity characteristic values. The left panel of Fig. 6 shows the map of the soil texture for the orbits covering Australia on 1 December 2010. The right panel shows the number of SMOS observations for each soil texture type. This figure shows that for these orbits the soil is dominated by coarse and medium textures, but fine and medium-fine textures also make a significant contribution. The averaged r^2 and STD mean values of the 2^{nd}-order polynomial fitted curve to the observations per soil type are shown for the XX and YY polarisations in Fig. 7 and Fig. 8, respectively. Results are presented separately for ascending and descending orbits and for all angular bins used in this study. These figures show similar results for all types of soil texture, except for the very fine soil texture type, in particular for descending orbits. Although for this type of soil texture the statistics are significant according to the p-value test, the number of observations collected was very low (see Fig. 6 right), and therefore not representative of this texture type. There is a good fit of the polynomial regression model to the observations, slightly better for ascending orbits and exceeding $r^2 = 0.7$ when the observations are averaged in angular bins. The best scores were obtained when angular bins of 2 degrees were applied to the observations. The STD values were in agreement with the statistics presented in Table 1. This figure also shows the advantages of averaging the data in

bins of up to 2 degrees, reducing the noise level by between 2.1 K and 3 K, depending on the continent, and similarly for ascending and descending orbits, as well as for both polarisations. Similar figures were obtained for North America and South America. For North America, the correlation of the observations with the polynomial regression model were lower for all soil types, which was also due to larger soil heterogeneities of North America compared to Australia. However, after binning up to 2 degrees the levels of noise were quite close to those of the Australia case, being slightly lower for descending orbits (not shown). While for North America these results showed a slight trend to decrease the noise of the observations with decreasing the size of the soil particles, the opposite trend was observed for South America. Therefore, these results do not provide any particular evidence of any type of soil texture over which observations are noisier than over the others, and all of them exhibit the same characteristics in terms of r^2 and STD statistical values.

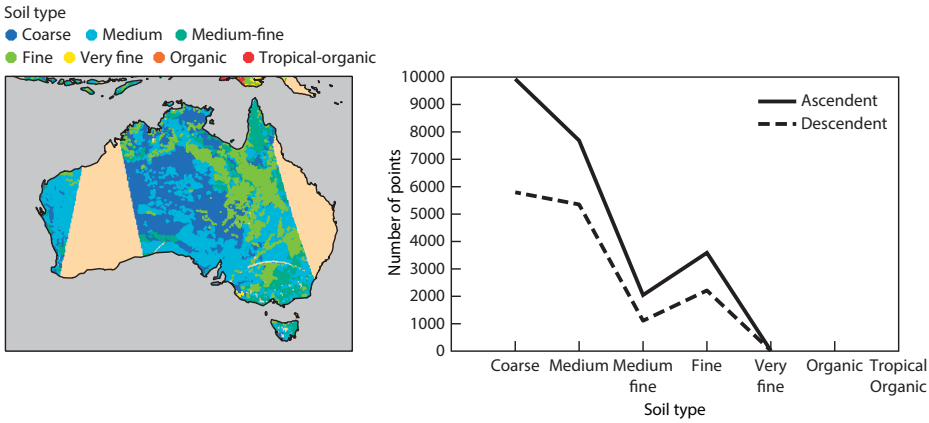

Figure 6: Soil type map (left) and number of observations per soil type (right) for ascending and descending orbits on 1 December 2010, in Australia.

4.2 Sensitivity to vegetation cover type

The vegetation cover type was also investigated as a possible factor influencing the amount of noise in the angular signature of the observations. As in section 4.1, statistics were computed independently for each type of vegetation cover used in H-TESSEL. It uses the classification of the Global Land Cover Characterization (GLCC) database which has been derived using one year of Advanced Very High Resolution Radiometer (AVHRR) data and ancillary information ((21); http://edcdaac.usgs.gov/glcc/glcc.html), the nominal resolution being 1 km. The vegetation cover types are split in high and low vegetation types. High vegetation types are evergreen needle-leaf trees, deciduous needle-leaf trees, deciduous broad-leaf trees, evergreen broad-leaf trees, mixed forest/woodland and interrupted forests. Low vegetation types include crops/mixed farming, short grass, tall grass, tundra, irrigated crops, semi-desert, bogs and marshes, evergreen shrubs and deciduous shrubs.

The semi-desert and tall grass types are the most representative of Australia. However, a significant amount of grid pixels over short grass, crops, ever-shrubs and inter-tropical forest types were also present in the satellite overpasses the dates used in this study. Australia obtained the best scores in terms of r^2 as a significant fraction of bare soil was commonly present in a pixel, as showed in section 2.3. Indeed, the angular signature of the observations was explained quite well by a 2^{nd}-order polynomial model, with the ascending orbits of the XX polarisation obtaining the best results (not shown). In terms of noise level, the results were very close for both types of orbit and slightly better for the XX polarisation. Both North and South America have a wider range of vegetation types over which significant correlation values are

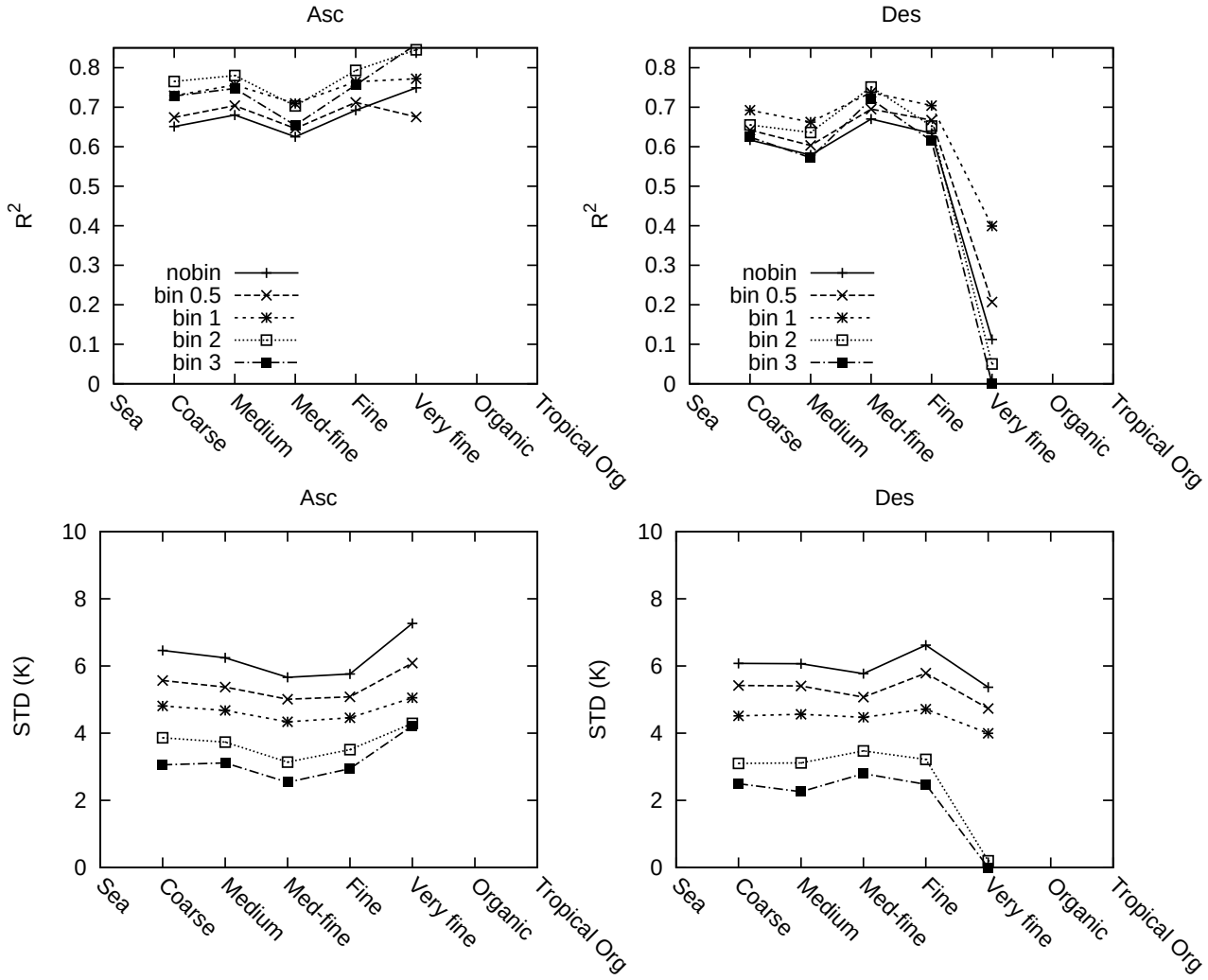

Figure 7: Mean coefficient of determination (r^2, top panel) and STD (in K, bottom panel) per type of soil texture for Australia, between SMOS brightness temperature and its 2^{nd}-order polynomial fit, for the XX polarisation and for ascending (left panel) and descending (right panel) orbits, on 1 December 2010.

available compared with Australia (see Fig. 9). For South America quite similar levels of noise were observed for each type of vegetation cover, as observed in Fig. 10 for XX polarisation and Fig. 11 for YY polarisation. No evidence of different behaviour between high or low vegetation types was found. Correlation values were a bit lower for the high vegetation type as the angular signature in this case was flatter and small deviations from the flat behaviour had a significant impact on the r^2 values. Noise levels were higher for the XX polarisation and slightly larger for ascending orbits. If very few number of significant observations were found for a vegetation cover type, then an anomalous behaviour was obtained. In this case, from the statistical point of view, the statistics are not representative of the whole class. See, for example, the abnormal high r^2 values for the evergreen needle-leaf trees class of South America in Figs. 10 and 11, or the very large noise found for irrigated crops of XX polarisation and ascending orbits.

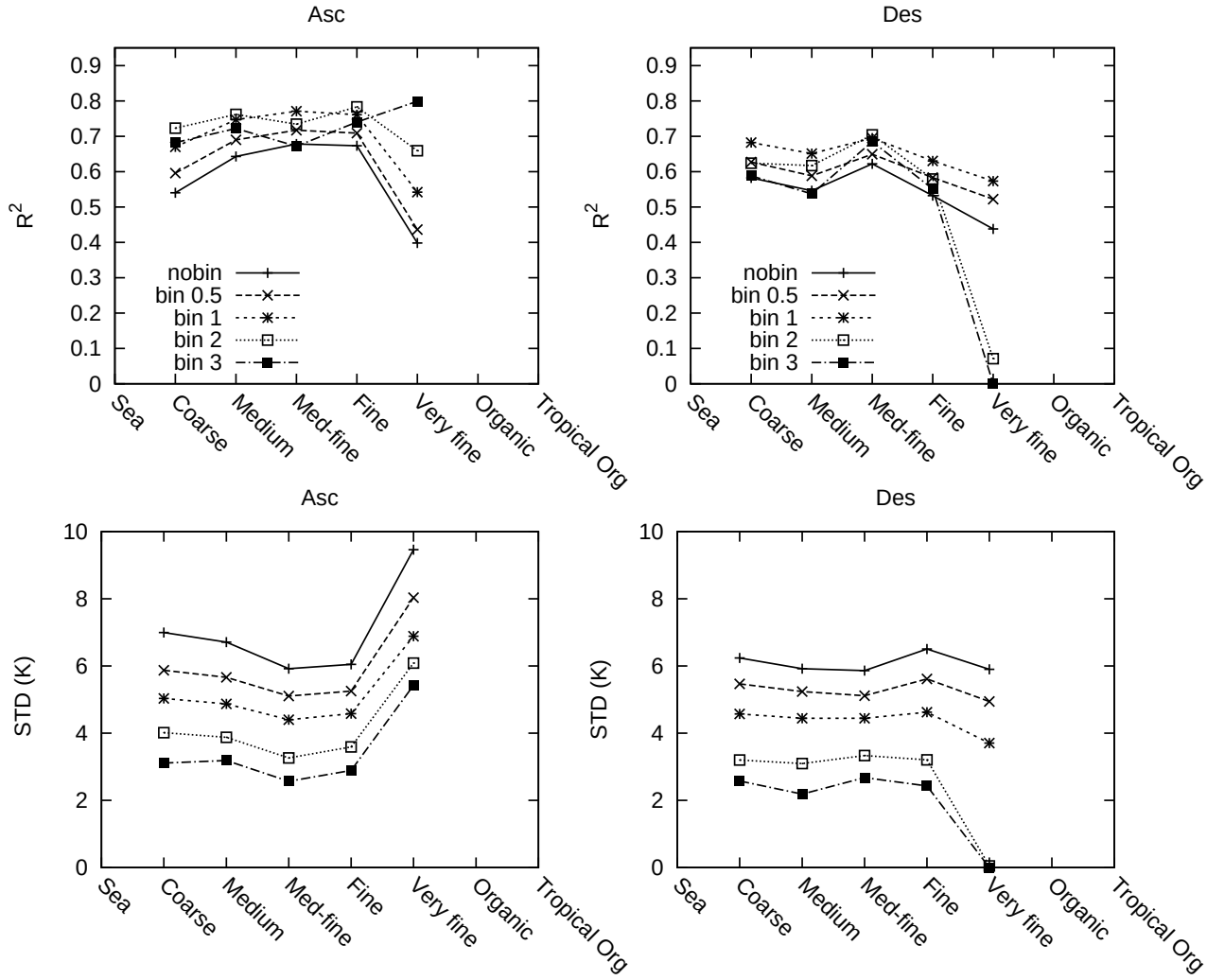

Figure 8: As in Fig. 7 but for the YY polarisation.

For North America a larger representation of evergreen forests was present. In this case slightly larger noise was found for ascending orbits than for South America (not shown), however the YY polarisation was noisier than the XX polarisation. The results obtained for the June case were similar for Australia and South America, with small differences reflecting the different state of development of the vegetation canopy and the changes on the soil cover during the two dates studied in this paper. The North America case exhibited a larger complexity, mainly due to the contrasted portion of land covered by snow between December and June. In the North America case, the ascending orbits presented larger noise when all the observations were used.

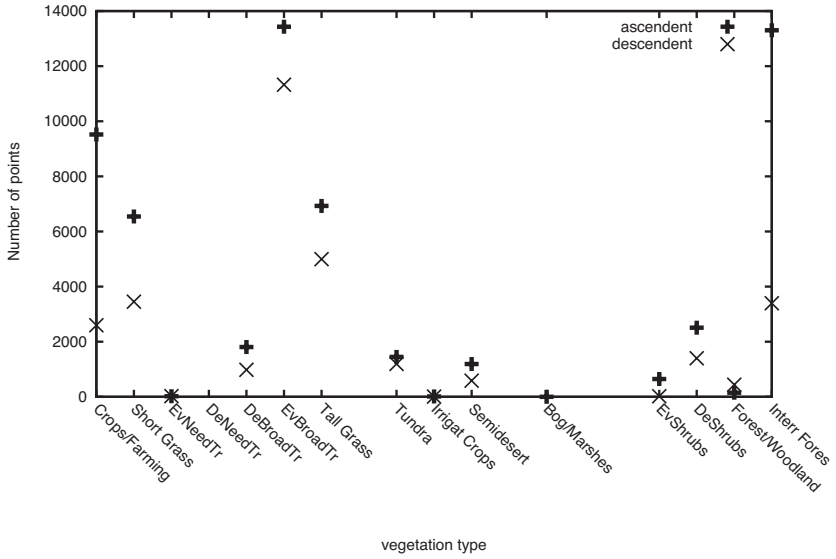

Figure 9: Number of SMOS observed brightness temperatures per vegetation biome type on 1 December 2010 in South America.

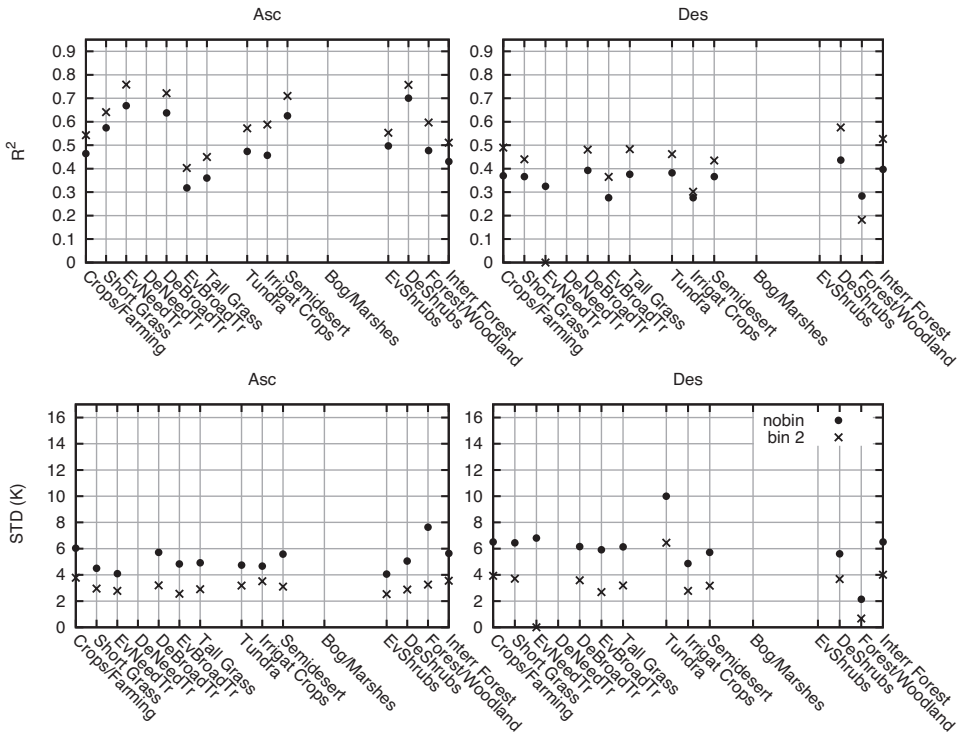

Figure 10: Mean coefficient of determination (r^2, top panel) and STD (in K, bottom panel) per type of vegetation in South America, between SMOS brightness temperature and its 2^{nd}-order polynomial fit, for the XX polarisation and for ascending (left panel) and descending (right panel) orbits, on 1 June 2011.

4.3 Sensitivity to the incidence angle

Data assimilation benefits most from those observations of higher quality and therefore it is important to understand whether some incidence angles are more affected by noise than others. In this context, the

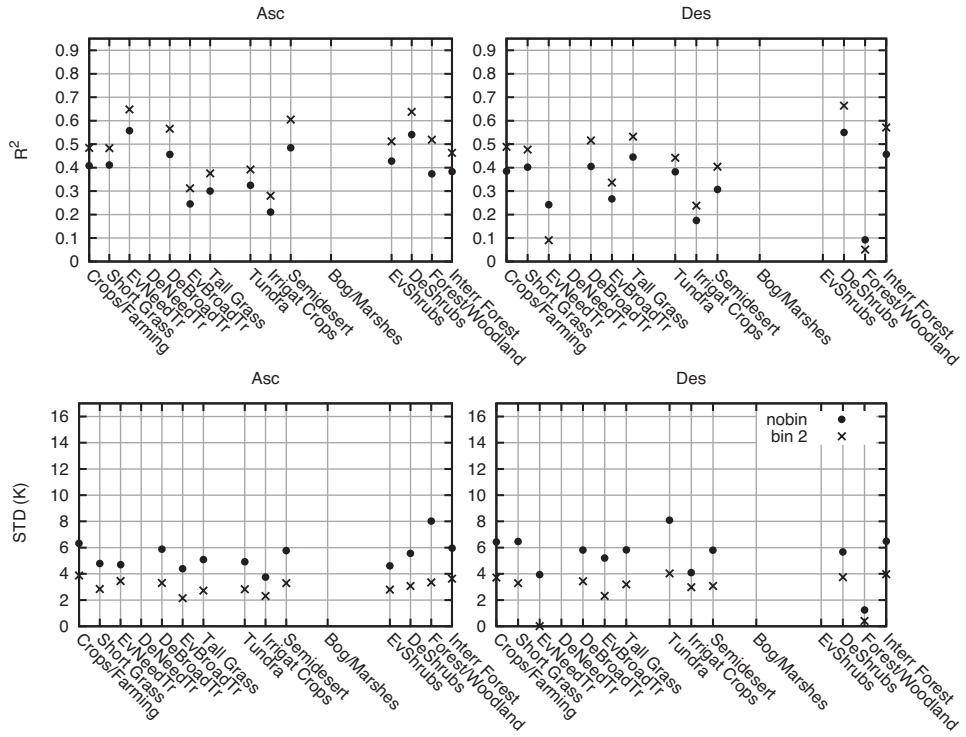

Figure 11: As in Fig. 10 but for the YY polarisation.

averaged standard deviation of the observations grouped in bins of 2 degrees was computed as a function of the incidence angle. Fig.12 shows the results separately per continent and per type of orbit. The left panels corresponds to the XX polarisation and the right panel to the YY polarisation. Overlapped on the XX polarisation plots, the number of observations collected for each angular bin of 2 degrees is shown. It is observed that the bin [42-44] degrees has in all cases the maximum number of observations, as 42.5 degrees is the incidence angle with the maximum number of views. In all cases, the smallest incidence angles were those affected with larger noise, as should be expected because for low incidence angles the signal to noise ratio is lower than for larger ones. A gradually increase in noise was also observed for the largest incidence angles, many of which were within the EA-FOV, an area of lower quality. Also, Australia showed the lowest level of noise, something which is consistent with previous findings, as Australia has a large portion of bare soil or lower vegetation density, and it is not affected by snow. The case of North America also exhibited larger noise than the others, which is a consequence of the snow cover during December.

4.4 Correlations with Radiometric accuracy

The radiometric accuracy of the observed brightness temperatures is related to the antenna, receiver and baseline errors (6). To some extent, the averaged radiometric accuracy of all the observations in a pixel should be related to the STD of the polynomial fitted curve of the observations in that pixel. Partly, the STD value should be explained by the averaged radiometric accuracy (which accounts for systematic errors), while the rest of the STD of the polynomial fit (under the hypothesis of the observations being explained by a 2^{nd}-order polynomial model) is associated with other noise contributions, as the angular noise or the noise associated to RFI signal contamination. Fig. 13 shows the STD of the fitted curve to the observations (after a 2-degree binning) as a function of the pixel averaged (over all observing

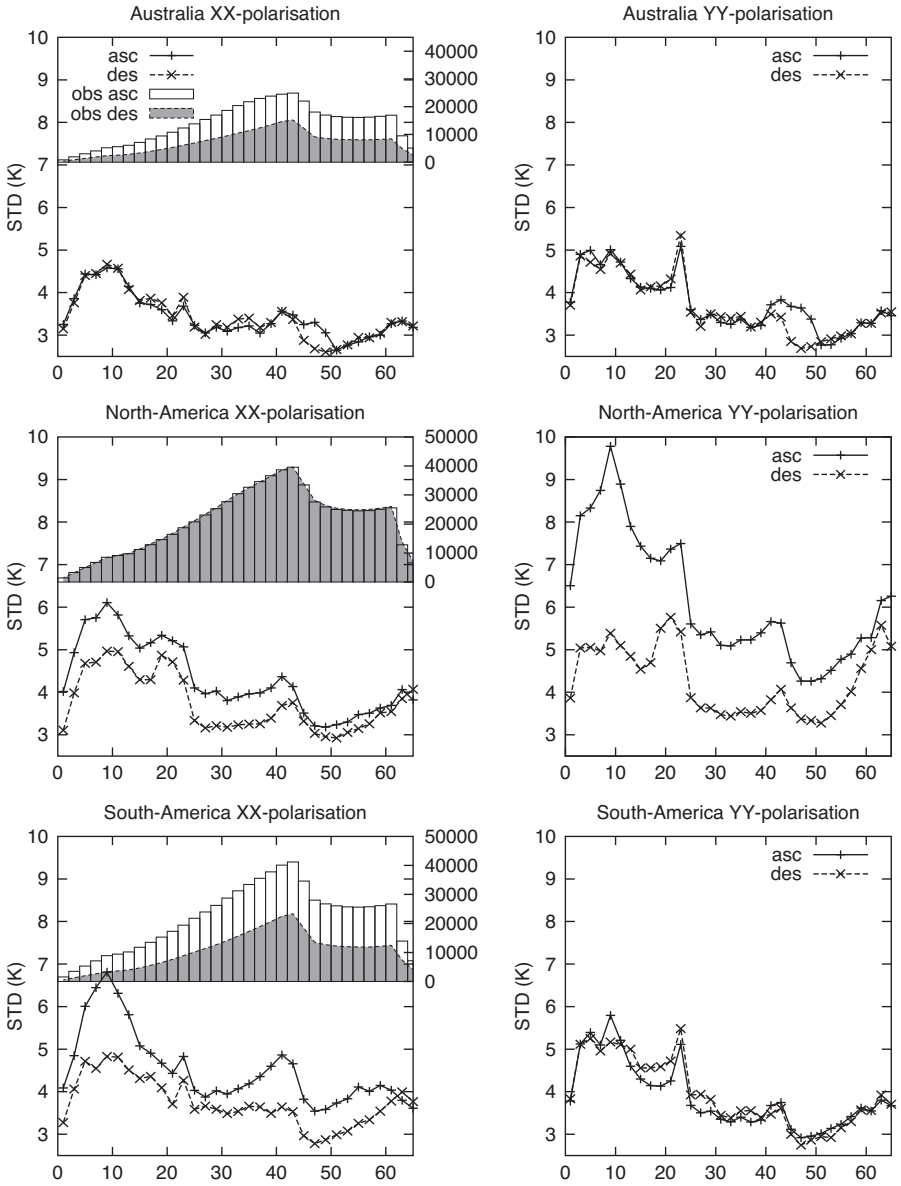

Figure 12: Averaged standard deviation of the observations in bins of 2 degrees as a function of the incidence angle of the observations, on 1 December 2010. Left panel is for the XX polarisation, right panel for the YY polarisation. Top figures are for Australia, middle figures for North America and bottom figures for South America. The number of observations as a function of the incidence angle is also overlapped on the left-panel figures, for ascending (empty vertical bars) and descending orbits (black vertical bars).

angles for that pixel) radiometric accuracy for 1 December 2010. As expected, in most cases pixels with the worse averaged radiometric accuracy are correlated with larger STD, reflecting the fact that the STD contains information of the observations radiometric accuracy. Also, as it has been discussed in previous sections, the STD for ascending and descending orbits are more similar over the Australian continent, compared with North and South America. Due to the instrument characteristics, ascending and descending views of a same surface pixel are not reconstructed from identical fields of view of the interferometric antenna. These differences are less significant if the viewed scene is more homogeneous. This could explain the more similar STD values for both ascending and descending orbits over Australia,

given the larger number of homogeneous views. It can also be observed that ascending orbits are clearly noisier than descending orbits in North and South America. In most cases, even after a 2-degree binning, the STD of the polynomial fit is greater than the averaged radiometric accuracy for ascending orbits. These differences between ascending and descending orbits are partially explained because the noise contributions to the signal (e.g. RFI contamination, open water bodies) are not necessarily the same for both type of orbits. Although not shown in this paper, when all the observations were used without any binning, the STD of the polynomial fit (containing information of the systematic errors and the angular noise) was always greater than the averaged radiometric accuracy.

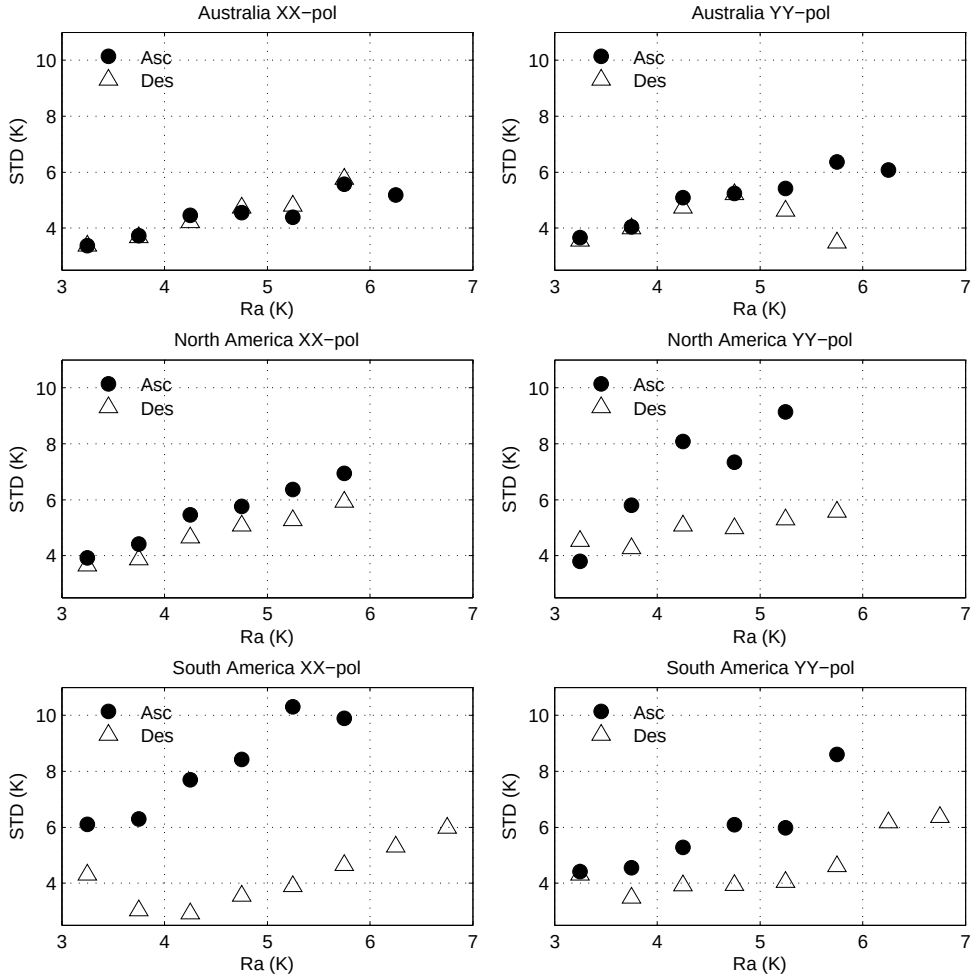

Figure 13: Mean STD of the observations fitted to a 2nd-order polynomial (with an angular binning of 2 degrees) as function of the pixel averaged observations radiometric accuracy (Ra), on 1 December 2010. Left panel is for the XX polarisation, right panel for the YY polarisation. Top figures are for Australia, middle figures for North America, bottom figures for South America. Results for the ascending orbits are plotted as filled circles, for the descending orbits as empty triangles.

5 Experimental case

The binning approach was tested in a real analysis case: SMOS brightness temperatures, at incidence angles of 30, 40 ad 50 degrees and pure XX and YY polarisations, were put through the ECMWF

Simplified Extended Kalman Filter (SEKF, (22; 23)) along with 2 m temperature and relative humidity observations, using a simple framework as detailed in (24). The resolution of the analysis was set to T159 spectral resolution (approximately 120 km). The period of the analysis spanned from 01 July to 31 August 2012. Two experiments were run: In exp-A, SMOS data were ingested in the SEKF, without binning the data. In exp-B, the data were binned and put through the analysis system using exactly the same conditions as in exp-A. The size of the angular bin was set to 2-degrees. The differences between both experiments can be attributed to the binning effect. In both experiments more than 25 million observations over land surfaces were available for use in the SEKF, after filtering and basic quality controls, as explained in (12). The left panel of Table 3 shows the percentage of rejected observations in exp-A and exp-B for XX polarization (Table 4 for YY polarization). In exp-A, more than 73% of the initial number of available observations were rejected for all regions and incidence angles, mainly due to the required criteria of one observation per model grid point, per incidence angle and polarization (12), as imposed by time and computational constraints. A maximum of 81.9% of the initial number of available observations were rejected in exp-A for use in the SEKF over Australia. However, in exp-B, the data were binned prior to the analysis, and in most cases less than 5% of observations were only rejected, frequently below 3% of the initial number. So on the contrary to exp-A, in exp-B very few useful observations are wasted and instead, indirectly through binning, the signal of a much larger amount of observations is used to analyse soil moisture (and ocean salinity). In average, more than 300.000 extra observations per day, at global scale, with averaged reduced noised are used to correct the water state of the soil. The right panel of Table 3 shows the mean standard deviation of the remaining observations of brightness temperatures at XX polarization (Table 4 for YY polarisation) used for the analysis, for the two months period, per incidence angle, polarisation and continent, with and without binning. For almost all cases, it can be observed a moderate but consistent decrease in the value of the mean standard deviation after binning. This decrease is below 1 K for 30 and 40 degrees, whereas is larger than 1 K for most cases at 50 degrees, where angular noise is stronger. The best case is Australia at 50 degrees and YY polarization, with a decrease of 1.78 K. This means a reduction close to 10% of the mean variability of the observations, which in an area free from RFI can be attributed to a reduction of the angular noise. Although not shown in this paper, it was checked that over certain ground stations, time series of soil moisture analysis in exp-B during the two-month period presented more dynamical stable behavior and lower increments of soil moisture, when compared to exp-A, which are also signs of better behavior of the retrievals. Longer experiments will be needed to confirm this improvement under all meteorological conditions.

6 Summary and conclusions

In this paper, the ability of the angular binning as a simple but effective method to reduce noise from the SMOS observed brightness temperatures, while retaining the signal, was quantified and demonstrated. The accuracy of soil moisture retrievals or numerical estimations of near-surface variables benefit from a dataset with reduced noise. Firstly, the angular noise of the observations was characterized by fitting all the observations to a polynomial regression model. The key statistical variables to be analysed are the coefficient of determination of the polynomial fit and the standard deviation of the residues to the fitted curve. They provide information about the representativity of the model used to explain the angular behaviour of the observations, and the associated noise. In order to obtain statistical representative values and to filter out local outliers (e.g. caused by local sources of RFI), mean values over continental areas were computed. A 2^{nd}-order polynomial regression model was chosen as reference model to characterize the angular behaviour of the observations. Higher-order polynomials should be avoided, as they better fit the noise to the regression model. Although a 2^{nd}-order polynomial is not perfect at characterizing the

angular distribution of SMOS brightness temperatures, it showed to be a reasonable good approximation in a wide variety of conditions. Secondly, the observations were averaged in bins of different size to reduce the angular noise of the observations. Finally, the effectiveness of the angular binning as a simple method to filter noise from the observations was validated, by using the same polynomial fit used to characterize the angular distribution of the observations.

It was found that averaging observed brightness temperatures in angular bins of different size effectively reduced the noise of the observations. The optimal bin size is 2 degrees, as for this bin the polynomial regression model characterizes better the angular signature of the observations while decreasing the noise. From a general perspective, this method has the potential to decrease noise from SMOS observed brightness temperatures by between 2 and 3 K. Other benefits are that the angular binning is computationally affordable and simple to implement in an operational system. It also complements data thinning approaches by contributing to reduce the volume of data in the original dataset. The latter makes it possible to investigate the influence of a single or several incidence angles in an analysis context, as more observations can be used at early stages of the analysis. In general, results were better for the XX polarisation, but some differences were found in North America, which were mainly due to the differences in the portion of soil covered by snow between the winter and summer cases. Although the XX polarisation is more sensitive to soil moisture variations, its larger dynamical range of brightness temperatures as a function of the incidence angle is not caused by a larger noise. It has greater skill to capture soil moisture variations than the YY polarisation. The difference in noise levels affecting the observations between both polarisations is reduced after binning the observations and, in most cases, varies from more than 1 K to a few tenths of kelvin when a 2 degree bin is applied. Near the coastlines spurious signals were observed, as the contribution from open water surfaces is embedded in the SMOS observations. The results presented in this study also indicate that, in general, ascending orbits are noisier than descending, but this conclusion may change if snow covered areas are included in the computations.

This study did not show any particular evidence of soil texture or vegetation cover type over which observations presented a noisier behaviour with the incidence angle. Slightly better representation of the low vegetation types by a 2^{nd}-order polynomial was shown, as over these pixels a greater sensitivity to the soil water content is present in the angular L-band signal. It was also found that incidence angles below 20 degrees are the noisiest ones, as they are affected by a lower signal to noise ratio, but in the other extreme, the largest incidence angles can present larger noise too. This information is important for data assimilation studies, as only the best observations should be assimilated. Also, the flat angular signature obtained for snow-covered areas and densely vegetated forests (therefore losing the sensitivity to soil moisture) produced lower correlation with the regression model and in many cases large noise values. For the soil moisture analysis these areas will also be masked out prior to assimilation, and a snow and dense forest mask will be applied to the observations. A good correlation between the observations radiometric accuracy and the STD of the polynomial fit to the observations was also found, reflecting the strong link between both variables. In this respect, the differences between ascending and descending orbits responds largely to the different areas observed by both types of orbits, and they are particularly strenghtned over very heterogeneous pixels. If a 2-degree binning is applied to the observations, the total estimated noise of a pixel can be reduced below the initial radiometric accuracy, at least for descending orbits. In the ECMWF SEKF, binning the data has also very significant consequences over the number of observations used to monitor the data and correct the state of the soil. Without binning, the signal of many useful observations is lost. A real case study showed moderate decrease in the observations standard deviation for a 2-month period, but is especially significant over large incidence angles, which are more affected with angular noise, as it would happen at very low incidence angles.

Finally, the introduction of RFI and quality flags in the SMOS NRT product will help to further enhance the efficiency of the binning approach, by rejecting contaminated or low-quality data before binning the observations, especially important in areas strongly affected by RFI as Europe or Asia.

Table 3: Global and regional statistics of SMOS data usage performance at XX polarisation, for exp-A (without binning, NB) and for exp-B (with binning, B). Left panel shows the percentage of observations rejected for use in the analysis system, per incidence angle. Right panel shows the mean standard deviation of the remaining SMOS brightness temperatures (in K).

	% of rejection						STD observations					
	30		40		50		30		40		50	
	NB	B	NB	B	NB	B	NB	B	NB	B	NB	B
Global	75.3	2.5	78.6	2.4	77.7	2.4	30.09	29.45	30.58	28.89	31.50	30.60
N.Amer	74.5	1.9	77.9	1.9	77.2	1.9	29.12	28.66	30.04	29.42	31.76	31.06
S.Amer	78.2	5.1	81.1	4.7	80.4	4.8	23.90	23.49	24.97	24.25	26.81	26.18
Africa	73.8	1.5	77.3	1.5	76.5	1.5	23.11	22.65	23.40	22.73	23.06	21.61
Europe	74.0	1.5	77.5	1.6	76.7	1.6	33.87	33.12	34.77	33.76	36.13	35.06
Australia	79.9	7.2	82.5	0.1	81.9	6.7	21.22	20.73	21.72	20.92	21.88	20.92

Table 4: As Table 3, but for YY polarisation.

	% of rejection						STD observations					
	30		40		50		30		40		50	
	NB	B	NB	B	NB	B	NB	B	NB	B	NB	B
Global	75.3	2.5	78.5	2.4	77.7	2.4	30.99	30.29	30.88	30.17	29.45	28.37
N.Amer	74.5	1.9	77.9	1.9	77.2	1.9	28.15	27.82	27.37	27.39	24.76	23.98
S.Amer	78.2	5.2	81.0	4.7	80.3	4.8	22.52	21.90	21.52	21.15	18.15	17.06
Africa	73.7	1.5	77.2	1.5	76.5	1.5	24.28	23.56	24.51	23.97	24.33	22.88
Europe	74.1	1.5	77.4	1.6	76.6	1.6	35.33	35.04	34.92	34.58	33.55	32.44
Australia	79.8	7.1	82.5	6.4	81.8	6.6	21.20	20.94	20.68	20.69	19.97	18.19

Acknowledgements

This work is funded under the ESA-ESRIN contract number 4000101703/10/NL/FF/fk. The authors would like to thank Matthias Drusch and Susanne Mecklenburg, both ESA staff, for their contribution in the project definition. Thanks also to Rob Hine for his support preparing the figures, and Joanne Jeppesen for the language and spelling suggestions, both ECMWF staff. Finally, thanks to Philippe Richaume and Yann Kerr (CESBIO) for their always fruitful discussions.

References

[1] Y. Kerr, P. Waldteufel, J.-P. Wigneron, S. Delwart, F. Cabot, J. Boutin, M. Escorihuela, J. Font, N. Reul, C. Gruhier, S. Juglea, M. Drinkwater, A. Hahne, M. Martin-Neira, and S. Mecklenburg, "The SMOS mission: New tool for monitoring key elements of the Global Water Cycle." *Proc. IEEE*, vol. 98, no. 5, pp. 666–687, 2010.

[2] Y. Kerr, P. Waldteufel, J.-P. Wigneron, J.-M. Martinuzzi, J. Font, and M. Berger, "Soil moisture retrieval from space: The soil moisture and ocean salinity (SMOS) mission." *IEEE Trans. Geosc. Remote Sens.*, vol. 39, no. 8, pp. 1729–1735, 2001.

[3] S. Pinori, R. Crapolicchio, and S. Mecklenburg, "Preparing the ESA-SMOS (Soil Moisture and Ocean Salinity) mission - Overview of the user data products and data distribution strategy," in *Microwave Radiometry and Remote Sensing of the Environment*, 2008.

[4] E.Anterrieu, "Brightness temperature map reconstruction from dual-polarimetric visibilities in synthetic aperture imaging radiometry," *IEEE Trans. Geosc. Remote Sens.*, vol. 46, no. 3, pp. 606 – 612, 2008.

[5] A. Camps, M. Vall-llosera, L. Batres, F. Torres, N. Duffo, and I. Corbella, "Retrieving sea surface salinity with multiangular L-band brightness temperatures: Improvement by spatio-temporal averaging," *Radio Science*, vol. 40, 2005, doi:10.1029/2004RS003040.

[6] A. Camps, J. Bara, F. Torres, I. Corbella, and J. Romeu, "Impact of antenna errors on the radiometric accuracy of large aperture synthesis radiometers," *Radio Science*, vol. 32, no. 2, pp. 657–668, 1997.

[7] E. Anterrieu and A. Camps, "On the reduction of the systematic error in imaging radiometry by aperture synthesis: a new approach for the SMOS space mission," in *Proceedings of IEEE MicroRad*, 2008, doi:10.1109/MICRAD.2008.4579462.

[8] A. Camps, M. Vall-llosera, I. Corbella, N. Duffo, and F. Torres, "Improved image reconstruction algorithm for aperture synthesis radiometers," *IEEE Trans. Geosc. Remote Sens.*, vol. 46, no. 1, pp. 146–158, 2008.

[9] J. Font, A. Camps, and J. Ballabrera-Poy, "Microwave aperture synthesis radiometry: Setting the path for (operational) sea salinity measurement from space," *Remote Sensing of European Seas*, pp. 223–238, 2008.

[10] J. Randa, J. Lahtinen, A. Camps, A. Gasiewski, M. Hallikainen, V. Leine, M. Martin-Neira, J. Piepmeier, P. Rosenkranz, C. Ruf, J. Shiue, and N. Skou, "Recommended terminology for microwave radiometry," National Institute of Standards and Technology, U.S. Department of Commerce, Tech. Rep., 2008, tech. Note 151.

[11] F. Torres, I. Corbella, A. Camps, N. Duffo, and M. Vall-llossera, "Error budget map to SRD (System Requirements Document) PRS. Project: Image Validation Support and SEPS Development, Validation and Delivery for SMOS PLM, Phase C/D, ESA Doc. Ref. SO-TN-UPCPLM-0007, version 7.0." Dept. of Signal Theor., Univ. Politecnica de Catalunya, Barcelona, Spain, Tech. Rep., 2005.

[12] J. Muñoz-Sabater, A. Fouilloux, and P. de Rosnay, "Technical implementation of SMOS data in the ECMWF Integrated Forecasting System," *Geosc. Remote Sens. Letters*, vol. 9, no. 2, pp. 252–256, 2012.

[13] K. Sahr, D. White, and A. J. Kimerling, "Geodesic discrete global grid systems cartography," *Cartography and Geographic Information Science*, vol. 30, no. 2, pp. 121–134, 2003.

[14] M. Suess, P. Matos, A. Gutierrez, M. Zundo, and M. Martin-Neira, "Processing of SMOS Level 1C data on a discrete global grid," in *IGARSS04 Proceedings*, 2004, pp. 1914–1917.

[15] J. Muñoz-Sabater, T. Wilhemsson, and P. de Rosnay, "Tech note- Part II- WP1200: Report on Data Thinning." European Centre for Medium-Range Weather Forecasts, Reading, United Kingdom, Tech. Rep., August 2011.

[16] J. Haseler, "Early delivery suite," European Centre for Medium-Range Weather Forecasts, Tech. Rep. 454, December 2004.

[17] M. Schervish, "P values: What they are and what they are not." *The American Statistician*, vol. 50, pp. 203–206, 1996, doi:10.2307/2684655.

[18] Y. Kerr, J. Font, P. Waldteufel, A. Camps, J. Bara, I. Corbella, F. Torres, N. Duffo, M. Vallilossera, and G. Caudal, "New radiometers: SMOS-a dual pol L-band 2d aperture synthesis radiometer," in *Aerospace Conference Proceedings*, vol. 8, 2000, pp. 119–118.

[19] Y. Kerr and E. G. Njoku, "A semi empirical model for interpreting microwave emission from semi-arid surfaces as seen from space," *IEEE Trans. Geosc. Remote Sens.*, vol. 28, pp. 384–393, 1990.

[20] G. Balsamo, P. Viterbo, A. Beljaars, B. van den Hurk, M. Hirschi, A. Betts, and K. Scipal, "A revised hydrology for the ECMWF model: Verification from field site to terrestrial water storage and impact in the integrated forecast system," *Journal of Hydrometeorology*, vol. 10, pp. 623–643, 2009, doi: 10.1175/2008JHM1068.1.

[21] T. Loveland, B. Reed, J. Brown, D. Ohlen, Z. Zhu, L. Youing, and J. Merchant, "Development of a global land cover characteristics database and IGB6 DISCover from the 1 km AVHRR data," *International Journal of Remote Sensing*, vol. 21, pp. 1303–1330, 2000.

[22] M. Drusch, P. de Rosnay, G. Balsamo, E. Andersson, P. Bougeault, and P. Viterbo, "Towards a Kalman filter based soil moisture analysis system for the operational ECMWF Integrated Forecast System," *Geophys. Res. Lett.*, vol. 36, 2009, doi:10.1029/2009GL037716, 2009.

[23] P. de Rosnay, M. Drusch, D. Vasiljevic, G. Balsamo, C. Albergel, and L. Isaksen, "A Simplified Extended Kalman Filter for the global operational soil moisture analysis at ECMWF," *Quart J. Roy. Meteor. Soc.*, vol. 139, no. 674, pp. 1199–1213, 2013, doi: 10.1002/qj.2023.

[24] J. Muñoz-Sabater, P. de Rosnay, C. Albergel, L. Isaksen, A. Fouilloux, M. Drusch, S. Mecklenburg, P. Lopez, A. Agusti-Panareda, Y. Kerr, P. Richaume, E. Dutra, and G. Balsamo, "Assimilation of SMOS brightness temperature at ECMWF: Impact on the Surface and Atmospheric Field," in *ESA Living Planet Symposium*, Edinburgh, Scotland, 2013.